ACS APPLIED MATERIALS & INTERFACES

Research Article

www.acsami.org

# Guidance of Stem Cells to a Target Destination in Vivo by Magnetic Nanoparticles in a Magnetic Field

Jialong Chen,[†,‡] Nan Huang,[†,*] Baolong Ma,[§] Manfred F. Maitz,[†,⊥] Juan Wang,[†] Jingan Li,[†] Quanli Li,[†,§] Yuancong Zhao,[†] Kaiqin Xiong,[†] and Xin Liu[‡]

[†]Key Laboratory of Advanced Technologies of Materials, Ministry of Education, and [§]School of Life Science and Engineering, Southwest Jiaotong University, Chengdu 610031, China

[‡]College of Stomatology, Anhui Medical University, Hefei 230032, China

[⊥]Leibniz Institute of Polymer Research Dresden, Max Bergmann Center of Biomaterials Dresden, Dresden 01069, Germany

Supporting Information

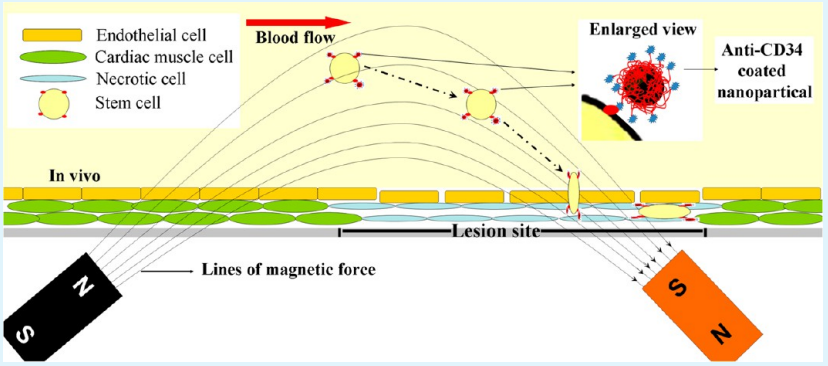


**ABSTRACT:** Stem cells contribute to physiological processes such as postischemic neovascularization and vascular re-endothelialization, which help regenerate myocardial defects or repair vascular injury. However, therapeutic efficacy of stem cell transplantation is often limited by inefficient homing of systemically administered cells, which results in a low number of cells accumulating at sites of pathology. In this study, anti-CD34 antibody-coated magnetic nanoparticles ($Fe_3O_4$@PEG-CD34) are shown to have high affinity to stem cells. The results of hemolysis rate and activated partial thromboplastin time (APTT) tests indicate that such nanoparticle may be used safely in the blood system. In vitro studies showed that a nanoparticle concentration of 100 $\mu$g/mL gives rise to a significant increase in cell retention using an applicable permanent magnet, exerting minimal negative effect on cell viability and migration. Subsequent in vivo studies indicate that nanopartical can specifically bind stem cells with good magnetic response. Anti-CD34 antibody coated magnetic nanoparticle may be used to help deliver stem cells to a lesion site in the body for better treatment.

**KEYWORDS:** *stem cell, magnetic nanopartical, poly(ethylene glycol), anti-CD34 antibody, homing, magnetic field*

## INTRODUCTION

Soon after the identification of stem cells (SCs), including hematopoietic stem cells, endothelial progenitor cells, cardiac stem cells, and bone marrow mononuclear cells, their use for regenerative therapies was explored. SCs have the capability to regenerate cardiomyocytes,[1−4] restore the function of ischemic organs by stimulating the re-endothelialization of injured blood vessels, and induce and modulate vasculogenesis and angiogenesis in areas with reduced oxygen supply.[5−8] The suitability of stem cells for the repair of myocardial tissue after myocardial infarction and for the repair of vascular injury have received much clinical attention.[9−11] Cellular therapies are increasingly applied in clinical trials; in recent years the use of stem cells as repairing modules in a compromised cardiovascular system has obtained modest success.[1,4,12] However, one of the current challenges in stem cell therapy is the localization of cells to the site of interest for the repair of damaged tissue. Developing methodologies that would target, monitor, and control cell guidance would therefore help current stem cell therapies make further progress.

Given their unique physical properties and their ability to function at the micrometer and submicrometer levels of biological interactions, magnetic nanoparticals (MNPs) are actively studied for use in the detection, diagnosis, and treatment of diseases such as cancer,[13] cardiovascular disease,[14] and neurological disease.[15] MNPs also lead to a remarkable decrease in the magnetic resonance imaging (MRI) parameter T2*, which makes possible the monitoring of the localization of

Received: January 28, 2013
Accepted: June 3, 2013
Published: June 7, 2013

  

nanoparticles noninvasively by MRI.[16,17] The magnetic properties of MNPs allow contactless mechanical manipulation by an applied magnetic field, which can be potentially applied in the local transport of magnetically tagged biological entities through the application of a magnetic field outside the body. Thus far, only one study has been reported regarding the guidance of magnetically tagged stem cells.[18] In that report, SCs were magnetically tagged by culturing the cells with MNPs overnight and allowing the endocytosis of MNPs by SCs. MNPs lack specificity for SCs, so SCs have to be isolated and expanded in culture for at least 2 weeks before tagging in vitro, making the procedure costly and time-consuming. Consequently, this method cannot be used for patients in need of emergency procedures. In the present study, we tested the administration of SC-specific MNP directly into the blood as alternative method to bind circulating SCs and allow direction of tagged SCs to target sites with the aid of applied magnetic field.

Cell targeting of MNPs has been very well studied for tumor location and site-specific drug delivery.[17] One promising approach for cell targeting, known as active targeting or specific targeting, is the conjugation of molecules, including proteins, peptides, aptamers, and small molecules, with high affinity and specificity to markers on the membrane of target cells. In general, stem cells are identified by the presence of three surface markers: CD34, CD133, and kinase insert domain receptor. Anti-CD34 antibody could therefore be immobilized onto MNPs for SC-specific targeting.

Nanoparticles have large surface-area-to-volume ratios and tend to agglomerate and adsorb plasma proteins. When nanoparticles agglomerate or are covered with adsorbed plasma proteins, they are quickly cleared by macrophages in the reticuloendothelial system before they can effectively accomplish their goal. Therefore, one possible approach to increase the circulation time of nanoparticles in the bloodstream is to coat the particles with hydrophilic polymers such as polyethylene glycol (PEG) to disperse the nanoparticles and minimize or eliminate protein adsorption.[19]

In this study, PEG and anti-CD34-coated $Fe_3O_4$ MNPs were prepared. To examine the concept experimentally, we first prepared and characterized these MNPs. We determined the affinity of MNPs to various cell types in the vascular systems in vitro and optimized stem cell capture conditions in terms of MNP concentration and magnetic field strength. We proceeded to test the use of MNPs for targeting SCs in vivo and the use of an applied magnetic field for the guidance of magnetically tagged SCs.

## EXPERIMENTAL SECTION

**Materials.** PEG-disuccinate (PEG-diacid, purity >98.5%) was purchased from Biomatrik Inc. Rabbit anti-CD34 polyclonal antibody was purchased from Beijing Biosynthesis Biotechnology Co., Ltd. FITC conjugated goat antirabbit IgG was purchased from Santa Cruz Biotechnology Inc. APTT kit was purchased from Shanghai Rongsheng Biotech Co., Ltd. FITC-conjugated rabbit anti-CD34 was purchased from Shanghai Haoran Biological Technology Co., Ltd. N-(3-Dimethyl-aminopropyl)-N′-ethylcarbodiimide hydrochloride (EDC), N-hydroxysuccinimide (NHS), and DAPI were purchased from Sigma-Aldrich. All the other reagents used in the experiments were of highest analytical purity (>99.9%)

**Synthesis and Characterization of PEG and Anti-CD34-Coated MNPs.** PEG-coated MNPs were synthesized following a simple two-step coprecipitation approach.[20] Initially, 0.10 g of $FeCl_2{\cdot}4H_2O$ and 0.27 g of $FeCl_3{\cdot}6H_2O$ were dissolved in 50 mL of deionized water under nitrogen protection. $PEG_{4000}$-diacid was added into the solution at a concentration of up to 2g/L. Ammonia was added dropwise to the solution and stirred for 10 min until the pH of the solution reached 10. Immediate color change from dark orange to black occurred with particle formation. Stirring was continued further for 60 min at 70 °C. PEG-coated nanoparticles, denoted as $Fe_3O_4$@PEG, were separated by magnetic decantation using a permanent magnet, and washed with deionized water several times. Bare $Fe_3O_4$ nanoparticles, denoted as $Fe_3O_4$, were prepared by the same method, but without the addition of $PEG_{4000}$-diacid into the solution. $Fe_3O_4$@PEG were ultrasonically dispersed in 20 mL of deionized water containing 100 mg of MES, 20 mg of EDC, and 15 mg of NHS for 60 min at 37 °C, separated by magnetic decantation, and washed with deionized water twice. $Fe_3O_4$@PEG with active carboxy groups was dispersed in 20 mL of PBS (pH 7.4) containing rabbit anti-CD34 polyclonal antibody in an orbital shaker incubator (37 °C, 80 rpm) for 4 h, separated by magnetic decantation, and washed with deionized water several times. Anti-CD34 coated nanoparticles denoted as $Fe_3O_4$@PEG-CD34 were also obtained.

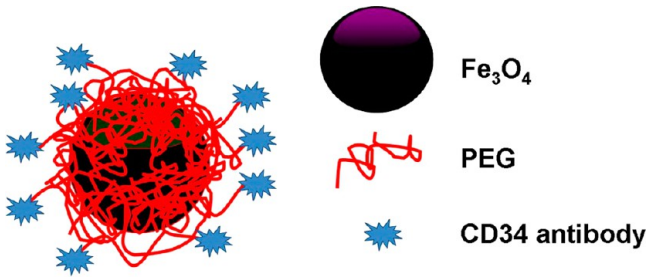


**Figure 1.** Ideal reaction scheme for the modified magnetic nanoparticles.

To investigate the nature of the chemical bond under ambient conditions, we recorded the FTIR spectra of MNPs in the 4000 to 400 $cm^{-1}$ range by the KBr pellet method using a Nicolet ST-IR20SX. Thermal stability was determined by thermogravimetric analysis (TGA, NETZSCH STA449C, Jupiter, Germany). TGA thermograms (TG) were measured for 20 mg of powder samples at a temperature range of 30 to 500 °C at a heating rate of 20 °C/min under nitrogen atmosphere. Due to high cost, anti-CD34 was substituted with bovine serum albumin (BSA) for $Fe_3O_4$@PEG-CD34 preparation in this analysis. X-ray diffraction patterns (XRD) of the MNPs were recorded with a Philips X'Pert Pro diffractometer using Cu K$\alpha$ ($\lambda$ = 1.5406 Å) radiation. BSA was also used for this analysis instead of anti-CD34. The shape of MNPs was determined using transmission electron microscopy (TEM) (JEM-2010, JEOL, Japan). The size distribution of the MNPs in Dulbecco's modified Eagle's medium (DMEM) (Gibco BRL, USA) culture medium containing 10% new born calf serum (NBCS) was obtained using a Malvern Nano ZS90 laser particle size analyzer. The Zeta potential of MNPs in deionized water (pH 6.5) was determined with a Zeta Potential Analyzer from Brookhaven Instruments Corporation. The magnetic properties (VSM) of MNPs were recorded in a vibrating sample magnetometer (Lake Shore 7410, Lake Shore Cryotronics, America). Magnetization values were normalized to the mass of the nanoparticles to determine the specific magnetization (emu per gram of particles).

The presence of anti-CD34 on the surface of MNPs was confirmed by immunofluorescent staining[21] as follows: (1) MNPs were immersed in 1% BSA solution for 30 min to block nonspecific adsorption, separated by magnetic decantation using a permanent magnet, and resuspended with deionized water; (2) 200 uL of FITC-conjugated goat antirabbit IgG (1:100) was added to the suspension, incubated for 1 h at 37 °C, separated by magnetic decantation, and washed with deionized water for 5 min three times; (3) The MNPs were immediately examined under a fluorescence microscope (LEICA DMRX Polarization microscope, Leica Germany).

**Isolation and Culture of SCs, ECs, SMCs, and Macrophages.** Mononuclear cells were separated by density gradient centrifugation (1800/min, 20 min) from the bone marrow of the femur of SD rats (Dashuo Co., Ltd., Chengdu). Without further purification steps, mononuclear cells were cultured in DMEM culture medium containing 20% NBCS, 10 ng/mL VEGF, 10 ng/mL SCF, penicillin (100 U/mL), and streptomycin sulfate (100 U/mL) at 37 °C under 5% $CO_2$. Cells were replenished with fresh medium every third day and subcultured regularly after adherent cells reached about 80% confluence. SCs were characterized by the expression of CD34 membrane protein by immunofluorescence.[22]

Endothelial cells (ECs) derived from human umbilical vein were isolated and cultured as subsequently described. The human umbilical cord was cannulated and washed thoroughly with PBS to remove the blood inside the lumen. Type II collagenase (Gibco BRL, USA) at 0.1% concentration in Medium 199 (M199) was introduced and incubated at 37 °C for 10 min. Detached cells were washed in serum-free medium and collected in complete M199 containing 10% fetal calf serum (FCS, Gibco BRL), 50 μg/mL EC growth factor (ECGF, Sigma), 100 μg/mL heparin, 20 mmol/L HEPES, 2 mmol/L L-glu, penicillin (100 U/mL), and streptomycin sulfate (100 U/mL), at 37 °C under 5% $CO_2$. Cells were replenished with fresh medium every third day and subcultured regularly after adherent cells reached about 80% confluence. The 3 third generation of ECs was used in the evaluation.

Human umbilical artery smooth muscle cells (SMCs) were isolated from newborn umbilical cord as described previously.[23] Cells in passages 2−5 were used. The SMCs were cultured in DMEM culture medium containing 10% NBCS, penicillin (100 U/mL), and streptomycin sulfate (100 U/mL) at 37 °C under 5% $CO_2$. Cells were replenished with fresh medium every third day and subcultured regularly after adherent cells reached about 80% confluence.

Peritoneal macrophages from SD rat were sterile harvested by flushing the peritoneum with 10 mL cold DMEM. Cells were centrifuged (1200 rpm, 5 min) and resuspended in DMEM containing 10% FBS.[21] The principal sensitivity of the used anti-CD34 antibody has been shown above by the reaction to stem cells.

**Ability of Nanoparticles to Target to SCs In Vitro.** To demonstrate the ability of MNPs to target SCs, four cell types were used: bone marrow-derived stem cells, peritoneal macrophages, endothelial cells, and vascular smooth muscle cells; two types of MNPs were used. The four cell types were suspended at a final concentration of $5 \times 10^4$/mL in DMEM. A cell suspension of 1 mL volume was added to each well in a 24-well tissue culture plate and incubated (37 °C, 5% $CO_2$) for 24 h. Media was withdrawn and adherent cells at the 24-well plate were incubated with serum-free DMEM medium containing 100 μg/mL MNPs for 5 min. The medium was aspirated and nonadherent MNPs in the wells were removed by washing with PBS. Cells without MNPs were used as control. Cells were fixed with 4% paraformaldehyde for 15 min and washed with PBS three times. The iron-sensitive Prussian blue (PB) staining was performed by incubating fixed cells in a mixture of 3% potassium ferrocyanide and 6% HCl (Perl reagent for PB staining) for 30 min. Cells were washed and counterstained with crystal violet, and observed by light microscopy for assessment of the ability of nanoparticles to target cell types of interest in vitro. Cells exhibiting blue particles were considered to be the target of MNPs.

**Influence of MNP Concentration on the SC Capture Effect.** SCs suspension at a density of $5 \times 10^4$/mL incubated with anti-CD34-coated MNPs at a concentration of 20, 100, or 500 μg/mL for 5 min in a 24-well flat-bottomed plate. A 300mT magnetic field was applied for 30 s at the bottom of the plate. Then, the suspension was removed, and every well was washed with PBS five times. An SC suspension without MNPs served as a control. The magnetic field was maintained in the process.

To demonstrate the viability and proliferation of the captured cells, we cultured the cells remaining in the well without magnetic field for 12 h at 37 °C in 5% humidified $CO_2$, washed them, and then stained them with crystal violet. The viability and proliferation of these cells were investigated by the Cell Counting Kit-8 (CCK-8, Sigma-Aldrich) after incubation for 1 and 3 days. The medium was removed and the wells were washed twice with PBS. Subsequently, 350 μL fresh DMEM culture medium containing 5% NBCS and 10% CCK-8 reagent was added to each of the wells, which were incubated at 37 °C for 3 h in standard culture conditions. Each of these solutions at 200 μL volume was analyzed for absorbance at 450 nm in a microplate reader. All proliferation experiments were performed in quadruplicate.

**Influence of MNP on the Viability and Migration of SCs.** After determining the optimal concentration of MNPs, the effect of anti-CD34-coated MNPs at this concentration on the viability and migration of SCs was investigated. SC suspension at a density of $5 \times 10^4$ /mL was added to each well in a 24-well tissue culture plate and incubated (37 °C, 5% $CO_2$). After 24 h of culture, the supernatant was discarded by aspiration, and fresh DMEM medium containing MNP (100 μg/mL) was added to each well (400 μL/well), whereas fresh DMEM medium without MNP served as control. After 5 min of incubation, the suspension was removed and each well was washed with PBS five times. The magnetic field was maintained in the process. Fresh DMEM medium containing 10% NBCS was added to each well at 1 mL volume and incubated (37 °C, 5% $CO_2$).

The viability of stem cells was investigated by CCK-8 assay after incubation for 1 and 3 d. Stem cell migration was investigated after SCs formed a confluent monolayer on the wells. With the guidance of a sterilized ruler, the tip of a 200 μL plastic pipet was used to gently scratch the confluent cell layer to create scarification. All cells were cultured for 1 and 3 days. After further rinsing, fixing, and immunofluorescent staining of actin,[22] SCs that have migrated into the scarification were observed under a fluorescence microscope by the expression of cytoskeleton actin.

**Influence of Magnetic Field Strength on the SC Capture Effect.** After determining the optimal concentration of MNPs, the magnetic field strength, which is also a factor that influences the capturing effect of MNPs, was investigated. SC suspension at a density of $5 \times 10^4$ /mL was incubated with MNPs at a concentration of 100 μg/mL for 5 min in a 24-well plate. Then, a magnetic field of 0, 100, or 300 mT was applied for 5 min at the bottom of the plate. The suspension was removed and each well was washed with PBS five times. The remaining cells were cultured without magnetic field for 12 h, washed, and stained with crystal violet. Meanwhile, the viability of the remaining cells in the well was investigated by CCK-8 assay.

**Hemolysis Rate Test.** MNPs at a concentration of 100 μg/mL were added into a solution of 2% fresh anticoagulated human blood and 98% physiological saline. They were then incubated at 37 °C for 1 h. MNPs were separated from the solution by the application of a 300 mT magnetic field at the bottom of the plate. After centrifugation at 3000 rpm for 5 min, the absorbance of the solution at 450 nm was recorded as $D_t$. Under the same conditions, a solution containing 2% fresh anticoagulated blood and 98% physiological saline without MNPs was used as negative reference, and a solution containing 2% fresh anticoagulated blood and 98% $dH_2O$ was used as positive reference. The absorbencies were recorded as $D_{nc}$ and $D_{pc}$, respectively. The hemolysis rate of the MNPs was calculated via the following formula

$$\alpha = \frac{D_t - D_{nc}}{D_{pc} - D_{nc}} 100\%$$

The term "hemolysis" is commonly used to describe the damage to red blood cells (erythrocytes) that result in the leakage of iron-containing hemoglobin protein into the bloodstream, which causes kidney problems, among others. Hemolysis is also an indicator of damage to other cells.

**APTT Test.** The activated partial thromboplastin time (APTT) is used as a general screening test for the detection of coagulation abnormalities in the intrinsic pathway and is commonly used to evaluate the anticoagulant properties of different biomaterials in vitro. To test the influence of MNPs on the APTT, platelet poor plasma (PPP) was prepared by centrifuging (3000 rpm, 15 min) citrate anticoagulated fresh human whole blood, after which it was added into the wells of a 24-well plate. MNPs were added to the PPP at a

concentration of 100 μg/mL and incubated at 37 °C for 30 min. Aliquots of 100 μL of PPP were taken, used for APTT test with a commercial test kit, and tests on a coagulometer KC 4A (Amelung, Germany) according to instructions of supplier.

**Ability of Anti-CD34-Coated MNPs to Capture SCs in Vivo.** Approval from the local laboratory animal committee was obtained for this study. To evaluate the ability of anti-CD34-coated MNP to capture SCs in vivo, we administered anti-CD34-coated MNP at a concentration of ∼2 mg/kg by intravenous injection to anaesthetized New Zealand rabbits. After 3.5 h, 2 mL of heparin (5 U/mL) was administered intravenously to prevent clotting, and blood was obtained by cardiac puncture. Blood samples were added into the wells of a six-well flat-bottomed plate and washed with PBS as a 300 mT magnetic field was applied at the bottom of the plate. The remainders were immunofluorescently stained with DAPI and for anti-CD34 as follows: (1) The remainders were immersed in 1% BSA in PBS for 30 min to block nonspecial adsorption, separated by magnetic decantation using a permanent magnet, and resuspended with PBS; (2) 200 μL of FITC conjugated rabbit anti-CD34 (20 μg/mL) was added to the suspension and incubated for 1 h. The remainders were separated by magnetic decantation and washed with PBS for 5 min three times; (3) 200 μL of DAPI (10 μg/mL) was added to the suspension and incubated for 5 min at 37 °C. The remainders were separated by magnetic decantation and washed with PBS for 5 min three times, and immediately examined under a fluorescence microscope. Meanwhile, mononuclear cells (SCs) were separated by density gradient centrifugation (1800 r/min, 20 min) with Ficoll-Paque (Amersham, UK) from whole blood collected in heparinized tubes as previously described.[24] The separated cells used as control were added into a six-well flat-bottomed plate and immunofluorescently stained with DAPI and for anti-CD34.

**Magnetic Guidance of SCs by Anti-CD34-Coated MNP.** This study was approved by the local laboratory animal committee. Anti-CD34-coated MNPs at a concentration of ∼2 mg/kg were intravenously administered to the blood system of anesthetic New Zealand rabbits to evaluate the magnetic response of anti-CD34 coated MNP in vivo. A 300 mT applied magnetic field was applied for 15 min at 15-min intervals at one of the femoral arteries. After 3.5 h, all femoral arteries were ligated, resected, and fixed in 4% paraformaldehyde. Femoral arteries of New Zealand rabbits without MNPs were ligated and resected. One of the arteries served as negative control and the other of arteries were injected with MNP suspension as positive control. All femoral arteries were placed into a 12-well flat-bottomed plate, fixed with 4% paraformaldehyde, and then analysis by magnetic resonance imaging (MRI) within 2 h.

MRI measurements were carried out on a 1.5-T Siemens Magnetom Avanto 32-channel "TIM" system. A volume coil was used for both transmission of radiofrequency pulses and signal reception. The following parameters were adopted for capturing the T2-weighted MR images in the experiments: slice thickness 1.6 mm, echo time of 113 ms, and repetition time of 4000 ms.

All experiments were performed for at least four times. All data were compared with one-way ANOVA tests using SPSS software to evaluate the statistical significance. Within the ANOVA analysis, Tukey multiple comparison test was performed to find significant differences between pairs. A probability value of less than 0.05 was considered statistically significant. Statistically significant differences ($p < 0.05$) in the figures were denoted with *.

## RESULTS AND DISCUSSIONS

The FTIR spectra of different kinds of MNP are shown in Figure 2. The FTIR measurements revealed that the vibration band of the metal−oxygen bond shifted from 579 $cm^{-1}$ for pure $Fe_3O_4$ to 587 $cm^{-1}$ for the PEG-coated MNP and anti-CD34-coated MNP, indicating that the O of PEG coordinated with that of Fe on the $Fe_3O_4$ surface.[25] The presence of new bands at 1394 and 1041 $cm^{-1}$ that correspond to the stretching of the $CH_x$ group, as well as at 1102 $cm^{-1}$ that corresponds to the stretching of C−O−C, confirm that PEG bonded to the surface of the $Fe_3O_4$ nanoparticles. Meanwhile, the vibration band of the C−O−C bond shifted from 1113 $cm^{-1}$ for pure PEG to 1102 $cm^{-1}$ for the nanoparticle. Studies have shown that the characteristic bands of PEG in the adsorbed state shifted to a lower-frequency region because the O from the C−O of PEG has coordination bond or strong interaction with Fe on the $Fe_3O_4$ surface.[26,27] Compared with PEG-coated MNP, the presence of the new band at 1233 $cm^{-1}$ that corresponded to primary amide III indicates that anti-CD34 antibody was linked to the PEG-coated MNP.

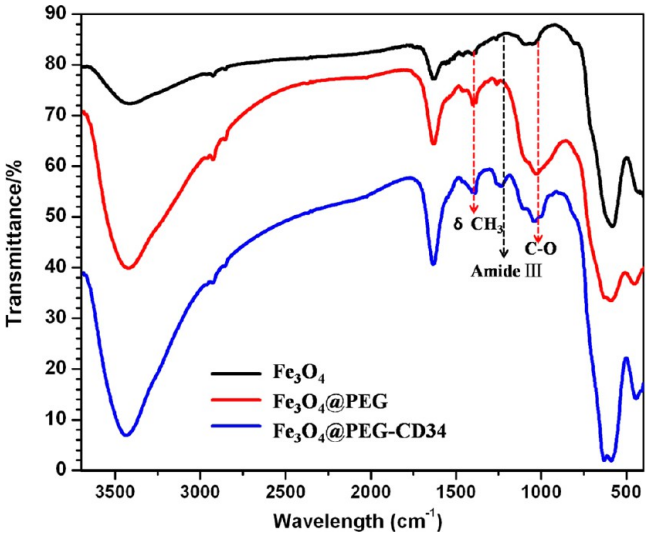


**Figure 2.** FTIR spectra of $Fe_3O_4$, $Fe_3O_4$@PEG, and $Fe_3O_4$@PEG-CD34.

To confirm the existence of PEG and protein (BSA instead of anti-CD34) on the $Fe_3O_4$ surface and quantify the proportion of organic and inorganic phases, we applied TG in a temperature range of 30−500 °C. The thermograms are presented in Figure.3. The TG curves of $Fe_3O_4$ showed a small weight loss of about 1% which is attributed to the evaporation of water molecules. A contiguous weight loss of $Fe_3O_4$@PEG and $Fe_3O_4$@PEG-BSA over a wide temperature range was

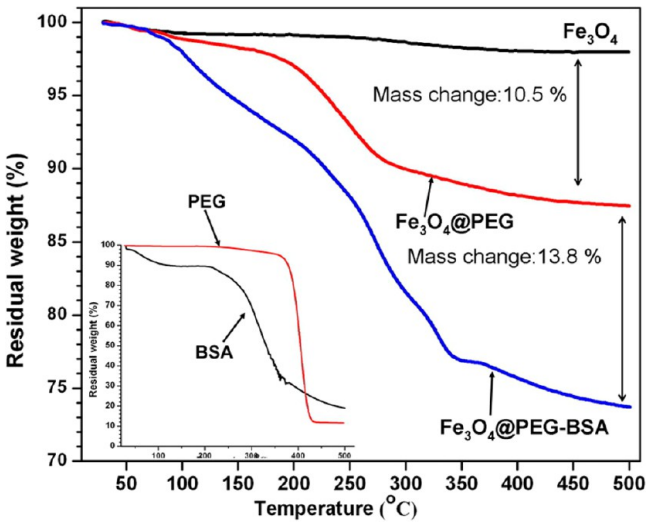


**Figure 3.** Thermograms of different kinds of magnetic nanoparticles. Subset: Thermograms of pure PEG and pure BSA.


dx.doi.org/10.1021/am400249n | ACS Appl. Mater. Interfaces 2013, 5, 5976−5985

observed. In agreement with a previous report,[28] pure PEG (as shown in the inset) combustion started at 340 °C and was completed at 420 °C. However, the degradation of PEG at the iron oxide particles started at a much lower temperature. This behavior originated from the fact that iron oxide particles behave as catalysts, thereby reducing the degradation temperature of PEG.[29] In the early state of slow degradation (<150 °C), a small weight loss of about 2% can be attributed to the loss of the water molecules. In the next state of fast degradation (150−300 °C) and slow degradation (>300 °C), a large weight loss of about 11% is attributed to the loss of the PEG molecules. Pure BSA (as shown in the inset) combustion started at 340 °C and was completed at 420 °C. The TG curves of pure protein showed a small endothermic weight loss of about 12% within the first 150 °C and 70% within 150 to 500 °C, corresponding to the loss of water and protein molecules. Thus, proteins have good water conservation. The degradation of $Fe_3O_4$@PEG-BSA showed a contiguous weight loss of about 25% because of the superposition of the loss of water, PEG and protein molecules. These results indicate that PEG and protein have been linked to $Fe_3O_4$ MNPs, and the weight percentages of $Fe_3O_4$ are 87 and 74% for $Fe_3O_4$@PEG and $Fe_3O_4$@PEG-BSA, respectively.

XRD measurements were performed with dried powder samples of all MNPs to identify the crystal phases. The XRD patterns are presented in Figure 4. All the observed diffraction

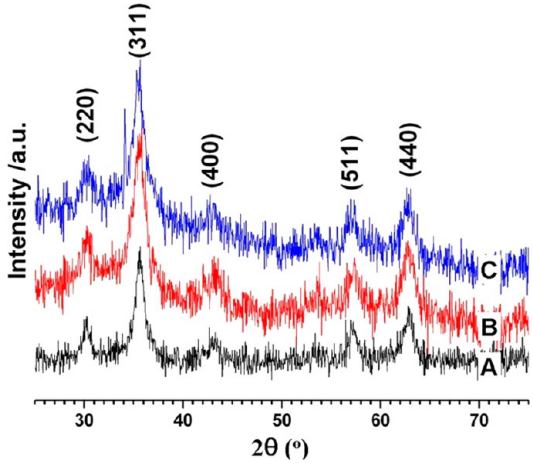


**Figure 4.** XRD spectra of (A) $Fe_3O_4$, (B) $Fe_3O_4$@PEG, and (C) $Fe_3O_4$@PEG-BSA.

peaks could be indexed by the cubic spinel phase of $Fe_3O_4$ (JCPDS No. 19−629) indicating a high phase purity of iron oxide. The characteristic peaks of PEG coated MNP and protein coated MNP did not change, indicating that the crystalline structure of the modified nanoparticles was not influenced by the additives. The broadening of the diffraction peaks of the PEG coated MNP and anti-CD34 coated MNP was observed because of the small crystallite size. The mean crystallite sizes obtained according to the Scherrer formula were about 23 ± 2, 18 ± 2, and 17 ± 2 nm, corresponding to $Fe_3O_4$, $Fe_3O_4$@PEG, and $Fe_3O_4$@PEG-CD34, respectively. The results indicate that the PEG coating process constrained the crystal growth, but did not affect the physical properties of the magnetite particles. PEG with a uniform and ordered chain structure is easily adsorbed at the surface of metal oxide colloids.[30] When the surface of the colloid adsorbs this type of polymer, the activities of the colloid will greatly decrease and the growth rate of the colloids in certain facets will be confined.[31] The crystallite sizes of all kinds of MNPs were smaller than 25 nm, so they possess superparamagnetism.[32]

The micrographs and size distribution histograms calculated are presented in Figures 5 and 6. $Fe_3O_4$ was observed to have more angular morphology, including squares, polygons, and parallelograms, with size lower than 30 nm. However, the size distribution of $Fe_3O_4$ in the DMEM medium containing 10% NBCS was above 1200 nm because eof severe aggregation (data not presented). After PEG coating, predominantly circular morphologies with size of ∼20 nm were observed from TEM, whereas the size distribution of the PEG-coated MNP in the DMEM medium containing 10% NBCS showed a wide range of ∼50−220 nm, with an average size of 106 nm. $Fe_3O_4$@PEG-CD34 had more nanoworm structures from TEM, with a size distribution in the DMEM medium containing 10% NBCS from ∼120−450 nm, with an average size of 190 nm. This observation indicates that PEG and anit-CD34 were linked to $Fe_3O_4$; a grafting of anti-CD34 caused the cross-linking of MNPs. The overall size of the MNPs used in vivo must be sufficiently small (<200 nm) to evade rapid splenic filtration but large enough (>5 nm) to avoid renal clearance.[17,33] Meanwhile, the filamentary[34] or nanoworm[35] structure of MNPs can prolong the circulating time in vivo. Thus, $Fe_3O_4$@PEG-CD34 could be used in vivo. The stability of $Fe_3O_4$@PEG-CD34 is the most important factor of the technique applied. Figure 6 shows that the size distribution of the anti-CD34 coated MNP in the DMEM medium containing 10% NBCS appeared to be almost unchanged up to 15 days in the dispersions, so the anti-CD34-coated MNPs are relatively stable.

A substantial understanding of the Zeta potential of nanoparticles would be helpful for understanding the validity of the preparation method. The Zeta potentials of $Fe_3O_4$, $Fe_3O_4$@PEG, and $Fe_3O_4$@PEG-CD34 in deionized water were −25 ± 4, −9 ± 5, and −2 ± 3 mV. This result indicates that PEG and anti-CD34 antibody was linked to $Fe_3O_4$.

MNPs exhibited good magnetic response and were easily attracted to a magnet as shown in Figure S1 in the Supporting Information. Under room temperature, the $M-H$ hysteresis curves of all kinds of nanoparticles measured with the magnetic field swept back and forth between +18 and −18 kOe as shown in Figure.7. No hysteresis behavior was observed, and the magnetization curves showed immeasurable coercivity and remanence. These observed properties are all typical features of superparamagnetic nanoparticles. The saturation magnetization ($M_s$) values of the nanoparticals obtained from the plot are 49.2, 41.2, and 24.8 emu/g for $Fe_3O_4$, $Fe_3O_4$@PEG and $Fe_3O_4$@PEG-BSA, respectively, which appeared considerably lower than that of the bulk magnetite (92 emu/g).[36,37] This result is partly attributed to the mass gain by PEG and BSA. If these $M_s$ values are normalized to the mass of the magnetite only, derived from the TG analysis in Figure 3, the Ms of $Fe_3O_4$ in $Fe_3O_4$@PEG and $Fe_3O_4$@PEG-BSA become 43.8 and 36.4 emu/g, which is still less than that of the Ms bulk $Fe_3O_4$. Reduced magnetization has been reported as a general observation for magnetite particles,[26,38−40] which is explained by the spin canting and the presence of disordered spins on the surface.[41,42] As the particle size decreases, the contribution of surface spins to the overall magnetization increases.[42] Another reason for the low magnetization values in the nanocomposites are the adsorbed PEG molecules bound to the surface via

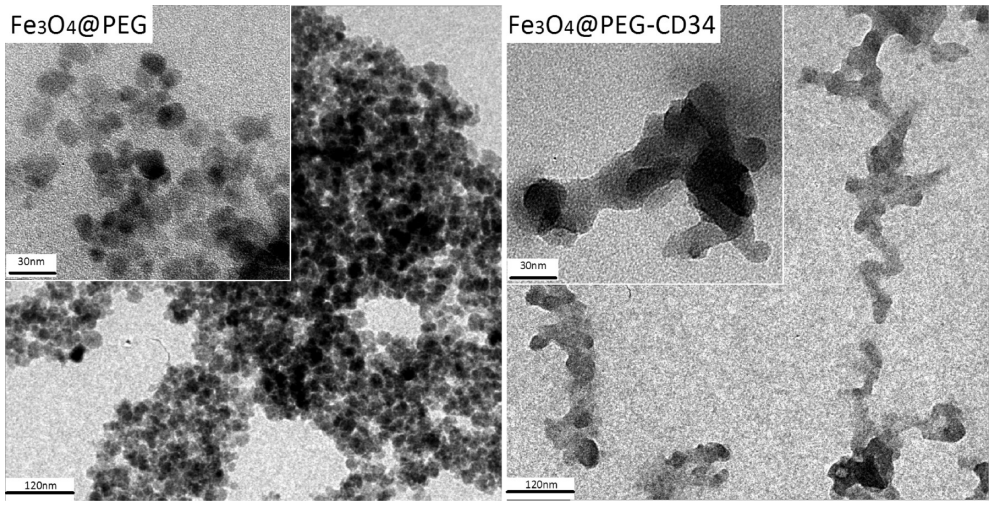


**Figure 5.** TEM micrographs of $Fe_3O_4$@PEG and $Fe_3O_4$@PEG-CD34.

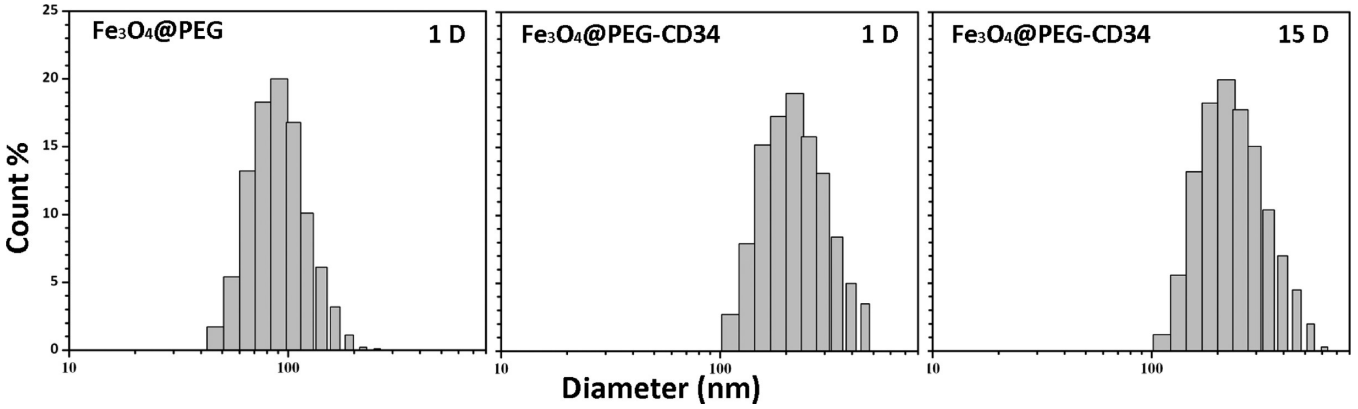


**Figure 6.** Size distribution of $Fe_3O_4$@PEG and $Fe_3O_4$@PEG-CD34 in the DMEM medium containing 10% NBCS for 1 and 15 days, respectively. The sizes of $Fe_3O_4$@PEG-CD34 appeared to be almost unchanged up to 15 days in the dispersions.

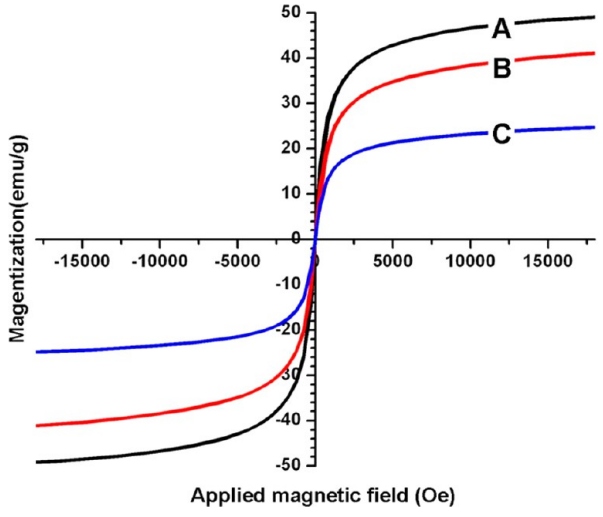


**Figure 7.** Magnetic hysteresis curves at room temperature for (A) $Fe_3O_4$, (B) $Fe_3O_4$@PEG, and (C) $Fe_3O_4$@PEG-BSA.

oxygen atoms as revealed from FTIR and weakens the super exchange interaction between Fe−O−Fe atoms close to the surface.[43] The overall magnetization of $Fe_3O_4$@PEG and $Fe_3O_4$@PEG-BSA indicates that PEG and protein have been linked to MNP.

The conjugation of the anti-CD34 antibody on the surface of the PEG-coated MNP was also confirmed by immunofluorescent staining. Figure 8 shows that $Fe_3O_4$@PEG-CD34 was stained strongly with FITC-conjugated goat antirabbit IgG, whereas no immunofluorescence was observed on $Fe_3O_4$@PEG. These results indicate that the anti-CD34 antibody has been linked to the PEG-coated MNP.

To capture the stem cells and deliver the cells to a target site with the aid of a magnetic field, the MNP must be highly specific for stem cells, and must show low cytotoxicity, good magnetic response, and good blood-compatibility.

To evaluate the specificity of $Fe_3O_4$@PEG-CD34 for stem cells versus other cells (control cells) that lack CD34 membrane protein expression, four cell types (i.e., peritoneal macrophages, smooth muscle cells, endothelial cells, and mononuclear cells from bone marrow (SCs)) were cultured with $Fe_3O_4$@PEG and $Fe_3O_4$@PEG-CD34, respectively, and then subjected to an iron sensitive Prussian blue (PB) staining. Light microscopy images are shown in Figure 9. The results showed that a notably higher amount of positive iron staining was observed only on the membrane of SCs cultured with $Fe_3O_4$@PEG-CD34, which proved that $Fe_3O_4$@PEG-CD34 possessed the characteristic to target SCs. Meanwhile, an extremely small quantity of positive iron staining was identified on the membrane of macrophages, which proved that $Fe_3O_4$@PEG-CD34 may be cleared by macrophages. No positive iron


dx.doi.org/10.1021/am400249n | ACS Appl. Mater. Interfaces 2013, 5, 5976−5985

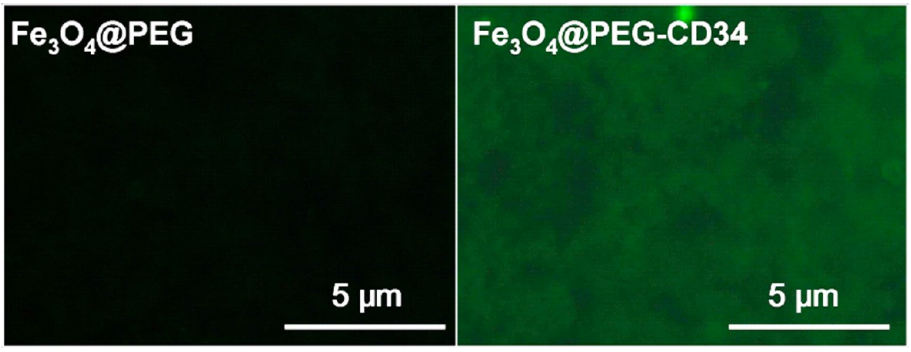


**Figure 8.** Fluorescent microphotographs of $Fe_3O_4$@PEG and $Fe_3O_4$@PEG-CD34.

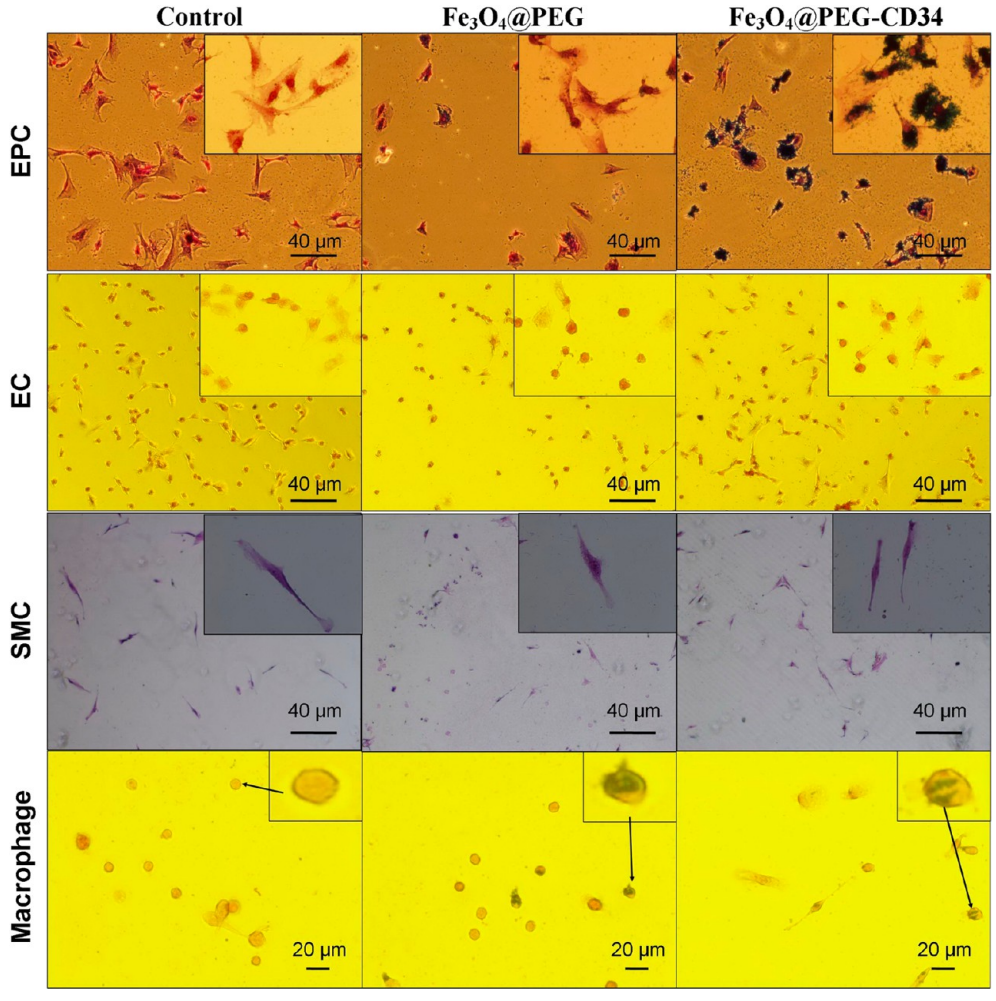


**Figure 9.** Prussian Blue stained microphotographs of cells incubatd with MNP.

staining was identified on the membrane of ECs and SMCs, indicating that the anti-CD34-coated MNP evaded the uptake by the reticuloendothelial system of ECs. These results indicate that anti-CD34-coated MNP will primarily bind SCs in the blood system.

The influence of the concentration of $Fe_3O_4$@PEG-CD34 on the number and the viability of captured stem cells are shown in Figures S2 and S3 in the Supporting Information. The results show that the number of captured cells on the sites where the magnetic field was applied increased with the concentration of MNPs, whereas few cells were observed in the control sites without magnetic field. The results indicated that $Fe_3O_4$@PEG-CD34 possessed the ability to capture SCs in the magnetic field. The highest number of spread cells was found in the group using 100 $\mu$g/mL rather than 500 $\mu$g/mL, indicating that a high concentration of $Fe_3O_4$@PEG-CD34 may injure the cells (see Figure S2 in the Supporting Information). Figure S3 in the Supporting Information shows that the proliferation of captured cells by different concentrations of $Fe_3O_4$@PEG-CD34 after 1 and 3 days of culture. The results also showed that the highest number of captured cells was found in the group using 100 $\mu$g/mL, and the captured cells showed good proliferative capacity. From the experiments, the concentration

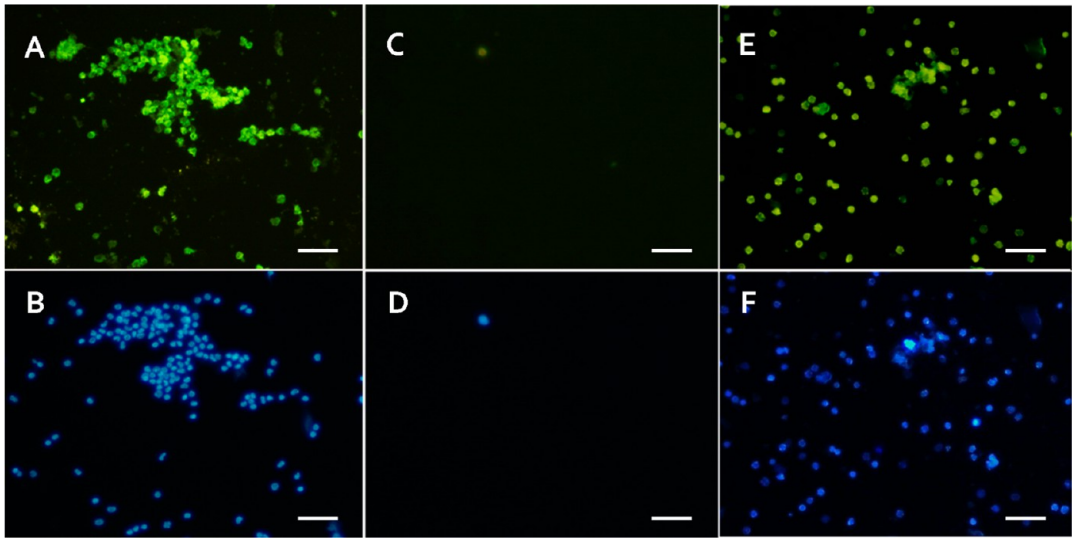


**Figure 10.** Mononuclear cells (SCs) as control, which were separated by density gradient centrifugation from whole blood of rabbit, were immunofluorescent stained with (A) anti-CD34 antibody and (B) DAPI. The compositions captured by $Fe_3O_4$@PEG from whole blood of rabbit were immunofluorescent stained with (C) anti-CD34 antibody and (D) DAPI. The compositions captured by $Fe_3O_4$@PEG-CD34 from whole blood of rabbit were immunofluorescent stained with (E) anti-CD34 antibody and (F) DAPI. Bar indicates 20 $\mu$m.

of anti-CD34 coated MNPs at 100 $\mu$g/mL was assumed to be the best choice for capturing stem cells.

After determining the optimal concentration of MNPs, we need to investigate the influence of anti-CD34-coated MNPs at this concentration on the viability and migration of SCs. Figure S4 in the Supporting Information shows that the viability of SCs had decreased to ~80% after incubation with anti-CD34 coated MNPs. The migration of SCs to the lesion sites is the most important means of postischemic neovascularization and vascular re-endothelialization. The effect of anti-CD34-coated MNPs on SC migration was analyzed when the SCs migrating from the periphery fully covered the whole scarification. The results revealed that the SCs incubated with MNPs had the same migration speed of SCs compared with the control (see Figure S5 in the Supporting Information). Thus, the migrating capacity of SCs incubated with MNPs (final concentration of 100 $\mu$g/mL) was not affected.

After identifying the optimal MNP concentration, the magnetic field strength, another major factor that influences the capture effect of MNPs, needs to be evaluated. The stem cells captured by anti-CD34 coated MNPs at various magnetic field strengths were cultured for 12 h. The adhered cells were then stained with crystal violet (see Figure S6 in the Supporting Information) and the number of stem cells captured by anti-CD34-coated MNPs were investigated by CCK-8 assay (see Figure S7 in the Supporting Information). The results show that the number of cells captured by anti-CD34 coated MNPs increased with magnetic field strength of up to 300 mT.

The intravenous application of nanoparticles requires good blood compatibility. The term "hemolysis" is commonly used to describe damage to red blood cells (erythrocytes) leading to the leakage of hemoglobin into the bloodstream For the anti-CD34 coated MNP a hemolysis rate of only 0.13% was determined, indicating the absence of hemolysis effect. The activated partial thromboplastin time (APTT) is used as a general screening test for the detection of coagulation abnormalities in the intrinsic pathway, and is also commonly used to evaluate the in vitro anticoagulation properties of different biomaterials. The APTT of plasma with 100 $\mu$g/mL anti-CD34 coated MNP was about 140 ± 8 s and was far beyond the APTT of PPP, which was about 39 ± 3 s. Anti-CD34-coated MNP will not lead to coagulation. The results of the hemolysis rate and APTT indicate that $Fe_3O_4$@PEG-CD34 may be used safely in the blood system.

Based on successful in vitro experiments, the anti-CD34 coated MNPs were used in subsequent in vivo experiments to capture SCs in the blood. First, the SCs separated by density gradient centrifugation from the whole blood of rabbit, were used as positive control to confirm that the captured compositions by anti-CD34 coated MNPs in the whole blood were stem cells, and were immunofluorescent stained with anti-CD34 antibody (Figure 10A) and DAPI (Figure 10B). The anti-CD34-coated MNPs were then injected via an ear vein into New Zealand rabbits. For negative control experiments, PEG-coated MNPs were intravenously injected into another New Zealand rabbit. After 3.5 h, blood was obtained from the animals and MNP bound cells were captured to a cell culture plate by magnetic field. The compositions captured by $Fe_3O_4$@PEG-CD34 were immunofluorescent stained with anti-CD34 antibody (E) and DAPI (F). The DAPI fluorescence staining verified that the captured compositions by $Fe_3O_4$@PEG-CD34 were cells, whereas the anti-CD34 fluorescence staining demonstrated that only $CD34^+$ cells were isolated. The results indicate that $Fe_3O_4$@PEG-CD34 possessed the ability to capture SCs in vivo.

To evaluate the magnetic response of anti-CD34-coated MNP in vivo, we injected anti-CD34-coated MNPs via an ear vein into New Zealand rabbits. A 300 mT applied magnetic field was utilized at one of femoral arteries. After 3.5 h, all femoral arteries were ligated, resected, and fixed. Femoral arteries without injected MNPs were ligated and resected. One of the arteries served as negative control, whereas the others were injected with MNP suspension as positive control. All femoral arteries were placed into a 12-well flat-bottomed plate, and T2*-weighted MR images of vessels were used to evaluate the magnetic response of the anti-CD34-coated MNPs in vivo, as shown in Figure 11. The signals in the positive control decreased greatly and were dark, so the femoral artery was

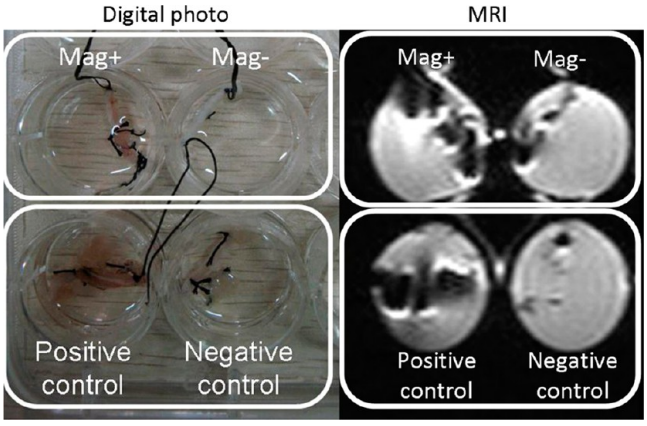


**Figure 11.** Digital photo (left) and MRI (right) of the femoral arteries. Anti-CD34-coated MNPs were injected via an ear vein into New Zealand rabbits. Up to 300 mT of magnetic field was applied on the femoral arteries (Mag+), whereas no magnetic field was applied on the other (Mag-). After 3.5 h, all femoral arteries were ligated, resected, and then fixed with paraformaldehyde. Femoral arteries of the New Zealand rabbits without MNPs were ligated and resected. One of the arteries served as negative control, whereas the other arteries were injected with MNP suspension as positive control.

clearly distinguished from the surrounding solution. Meanwhile, the negative control did not extinguish the signals and could not be distinguished from the surrounding solution. For the experimental group, the femoral artery exposed to a magnetic field (Mag+) showed greater signal suppression and appeared darker than the femoral artery without a magnetic field (Mag−). The results indicate that $Fe_3O_4$@PEG-CD34 in vivo is responsive to the applied magnetic field; it could be accumulated at the area where the magnetic field was placed and would not be cleared within 3.5 h. The applied magnetic field was added at 15-min intervals and high shear force was provided by the blood flow, so not all MNPs were drawn to the area of the magnetic field placed. The femoral artery without a magnetic field (Mag-) showed the existence of MNP.

## CONCLUSION

In this study, a new approach that could induce more stem cells to accumulate at the lesion sites for regenerating myocardial defects or repairing vascular injury was proposed. This new type of magnetic nanoparticle specifically binds SCs in the whole blood in vivo, and then delivers SCs to the lesion sites where a permanent magnet is applied. A new type of magnetic nanoparticle of $Fe_3O_4$@PEG-CD34 was successfully prepared using PEG and anti-CD34 antibody to modify $Fe_3O_4$. The results indicate that such MNP possesses good blood compatibility, could specifically bind stem cells, have good magnetic response, and helps deliver stem cells to the lesion sites. Therefore, this work must be continued to assess the therapeutic efficacy of $Fe_3O_4$@PEG-CD34 in vivo and to design better magnetic nanoparticles.

## ASSOCIATED CONTENT

### Supporting Information

Additional figures. This material is available free of charge via the Internet at http://pubs.acs.org/.

## AUTHOR INFORMATION

### Corresponding Author

*E-mail: nhuang@263.net. Tel/Fax: +86-28-87600625.

### Notes

The authors declare no competing financial interest.

## ACKNOWLEDGMENTS

This work was supported by Key Basic Research Program (2011CB606204), Natural Science Foundation of China (30831160509, 50971107, and 81201191). This work was also supported by Grants for Scientific Research of BSKY(XJ201232) from Anhui Medical University".

## REFERENCES

(1) Rodrigo, S. F.; Ramshorst, J.; Beeres, S. L.; Bax, J. J.; Schalij, M. J.; Atsma, D. E. *Curr. Pharm. Des.* **2011**, *17*, 3308−27.
(2) Reinlib, L.; Field, L. *Circulation* **2000**, *101*, E182−7.
(3) Ince, H.; Stamm, C.; Nienaber, C. *Curr. Treat. Options Cardiovasc. Med.* **2006**, *8*, 484−495.
(4) Hoover-Plow, J.; Gong, Y. *Vasc. Health Risk. Manage.* **2012**, *8*, 99−113.
(5) Hristov, M.; Erl, W.; Weber, P. C. *Arterioscler. Thromb. Vasc. Biol.* **2003**, *23*, 1185−1189.
(6) Woywodt, A.; Bahlmann, F. H.; De Groot, K.; Haller, H.; Haubitz, M. *Nephrol. Dial. Transplant.* **2002**, *17*, 1728−30.
(7) Szmitko, P. E.; Kutryk, M. J. B.; Stewart, D. J.; Strauss, M. H.; Verma, S. *Can. J. Cardiol.* **2006**, *22*, 1117−1119.
(8) Sata, M.; Saiura, A.; Kunisato, A.; Tojo, A.; Okada, S.; Tokuhisa, T.; Hirai, H.; Makuuchi, M.; Hirata, Y.; Nagai, R. *Nat. Med.* **2002**, *8*, 403−409.
(9) Mushtaq, M.; Oskouei, B. N.; Hare, J. M. *Circ. Res.* **2011**, *108*, 398−401.
(10) Heldman, A. W.; Zambrano, J. P.; Hare, J. M. *J. Am. Coll. Cardiol.* **2011**, *57*, 466−8.
(11) Asahara, T.; Murohara, T.; Sullivan, A.; Silver, M.; vanderZee, R.; Li, T.; Witzenbichler, B.; Schatteman, G.; Isner, J. M. *Science* **1997**, *275*, 964−967.
(12) Herrmann, J. L.; Abarbanell, A. M.; Weil, B. R.; Wang, Y.; Wang, M.; Tan, J.; Meldrum, D. R. *Ann. Thorac. Surg.* **2009**, *88*, 1714−22.
(13) Ferrari, M. *Nat. Rev. Cancer* **2005**, *5*, 161−71.
(14) Wickline, S. A.; Neubauer, A. M.; Winter, P. M.; Caruthers, S. D.; Lanza, G. M. *J Magn. Reson. Imaging* **2007**, *25*, 667−80.
(15) Corot, C.; Petry, K. G.; Trivedi, R.; Saleh, A.; Jonkmanns, C.; Le Bas, J. F.; Blezer, E.; Rausch, M.; Brochet, B.; Foster-Gareau, P.; Baleriaux, D.; Gaillard, S.; Dousset, V. *Invest. Radiol.* **2004**, *39*, 619−25.
(16) Bulte, J. W.; Kraitchman, D. L. *NMR Biomed.* **2004**, *17*, 484−99.
(17) Sun, C.; Lee, J. S.; Zhang, M. *Adv. Drug. Delivery Rev.* **2008**, *60*, 1252−65.
(18) Kyrtatos, P. G.; Lehtolainen, P.; Junemann-Ramirez, M.; Garcia-Prieto, A.; Price, A. N.; Martin, J. F.; Gadian, D. G.; Pankhurst, Q. A.; Lythgoe, M. F. *JACC Cardiovasc. Interventions* **2009**, *2*, 794−802.
(19) Gupta, A. K.; Gupta, M. *Biomaterials* **2005**, *26*, 3995−4021.
(20) Lee, J.; Isobe, T.; Senna, M. *J. Colloid Interface Sci.* **1996**, *177*, 490−494.
(21) Chen, J.; Cao, J.; Wang, J.; Maitz, M. F.; Guo, L.; Zhao, Y.; Li, Q.; Xiong, K.; Huang, N. *J. Colloid Interface Sci.* **2012**, *368*, 636−47.
(22) Chen, J.; Chen, C.; Chen, Z.; Chen, J.; Li, Q.; Huang, N. *J Biomed. Mater. Res. A* **2010**, *95A*, 341−349.
(23) Vadiveloo, P. K.; Stanton, H. R.; Cochran, F. W.; Hamilton, J. A. *Artery* **1994**, *21*, 161−181.
(24) Clarke, L. A.; Shah, V.; Arrigoni, F.; Eleftheriou, D.; Hong, Y.; Halcox, J.; Klein, N.; Brogan, P. A. *J. Thromb. Thrombolysis* **2008**, *6*, 1025−32.
(25) Ma, M.; Zhang, Y.; Yu, W.; Shen, H.-y.; Zhang, H.-q.; Gu, N.. *Colloids Surf., A* **2003**, *212*, 219−226.
(26) Ebubekir, K.; Huseyin, K.; Abdulhadi, B.; Muhammet S., T.; Sözeri, H. *Nano-Micro. Lett.* **2011**, *3*, 79−85.

(27) Mukhopadhyay, A.; Joshi, N.; Chattopadhyay, K.; De, G. *ACS Appl. Mater. Interfaces* **2011**, *4*, 142−149.
(28) Xiaotun, Y.; Lingge, X.; Choon, N. S.; Hardy, C. S. O. *Nanotechnology* **2003**, *14*, 624.
(29) Ünal, B.; Durmus, Z.; Baykal, A.; Sözeri, H.; Toprak, M. S.; Alpsoy, L. *J. Alloys Compd.* **2010**, *505*, 172−178.
(30) Huang, H. H.; Ni, X. P.; Loy, G. L.; Chew, C. H.; Tan, K. L.; Loh, F. C.; Deng, J. F.; Xu, G. Q. *Langmuir* **1996**, *12*, 909−912.
(31) Lee, J.; Isobe, T.; Senna, M. *J. Colloid Interface Sci.* **1996**, *177*, 490−494.
(32) Liu, X.; Kaminski, M. D.; Guan, Y.; Chen, H.; Liu, H.; Rosengart, A. J. *J Magn. Magn. Mater.* **2006**, *306*, 248−253.
(33) Ito, A.; Shinkai, M.; Honda, H.; Kobayashi, T. *J Biosci. Bioeng.* **2005**, *100*, 1−11.
(34) Geng, Y.; Dalhaimer, P.; Cai, S.; Tsai, R.; Tewari, M.; Minko, T.; Discher, D. E. *Nat. Nanotechnol.* **2007**, *2*, 249−55.
(35) Park, J. H.; von Maltzahn, G.; Zhang, L.; Schwartz, M. P.; Ruoslahti, E.; Bhatia, S. N.; Sailor, M. J. *Adv. Mater.* **2008**, *20*, 1630−1635.
(36) Han, D. H.; Wang, J. P.; Luo, H. L. *J Magn. Magn. Mater.* **1994**, *136*, 176−182.
(37) Sato, T.; Iijima, T.; Seki, M.; Inagaki, N. *J Magn. Magn. Mater.* **1987**, *65*, 252−256.
(38) Durmus, Z.; Kavas, H.; Baykal, A.; Sozeri, H.; Alpsoy, L.; Celik, S. U.; Toprak, M. S. *J. Alloys Compd.* **2011**, *509*, 2555−2561.
(39) Batlle, X.; Labarta, A. *J Phys. D: Appl. Phys.* **2002**, *35*, R15−R42.
(40) Murbe, J.; Rechtenbach, A.; Topfer, J. *Mater. Chem. Phys.* **2008**, *110*, 426−433.
(41) Berkowitz, A. E.; Lahut, J. A.; Jacobs, I. S.; Levinson, L. M.; Forester, D. W. *Phys. Rev. Lett.* **1975**, *34*, 594−597.
(42) Goya, G. F.; Berquo, T. S.; Fonseca, F. C.; Morales, M. P. *J. Appl. Phys.* **2003**, *94*, 3520−3528.
(43) Karaoğlu, E.; Baykal, A.; Deligöz, H.; Şenel, M.; Sözeri, H.; Toprak, M. S. *J. Alloys Compd.* **2011**, *509*, 8460−8468.